

Chiral solitons in spinor polariton rings

D. A. Zezyulin,¹ D. R. Gulevich,¹ D. V. Skryabin,^{1,2} and I. A. Shelykh^{1,3}¹*ITMO University, St. Petersburg 197101, Russia*²*Department of Physics, University of Bath, Bath BA2 7AY, United Kingdom*³*Science Institute, University of Iceland, Dunhagi 3, IS-107, Reykjavik, Iceland*

(Received 30 October 2017; revised manuscript received 29 March 2018; published 12 April 2018)

We consider theoretically one-dimensional polariton ring accounting for both longitudinal-transverse (TE-TM) and Zeeman splittings of spinor polariton states and spin-dependent polariton-polariton interactions. We present a class of solutions in the form of the localized defects rotating with constant angular velocity and analyze their properties for realistic values of the parameters of the system. We show that the effects of the geometric phase arising from the interplay between the external magnetic field and the TE-TM splitting introduce chirality in the system and make solitons propagating in clockwise and anticlockwise directions nonequivalent. This can be interpreted as a solitonic analog of the Aharonov-Bohm effect.

DOI: [10.1103/PhysRevB.97.161302](https://doi.org/10.1103/PhysRevB.97.161302)

Introduction. Topology of the potential is critical for the dynamics of a quantum particle since it defines connectivity of the available trajectories. Therefore changes in the topology of a system are often related to qualitative alternations of its physical behavior [1]. Quantum nonsingle connected structures, such as mesoscopic rings, reveal a rich variety of quantum-mechanical effects [2–4]. One prominent example is the famous Aharonov-Bohm effect [5,6] where the phase of a charged particle is influenced by the magnetic field, which is effectively zero at the particle's location. This results in magnetic-flux-dependent oscillations of the ring-confined particle energy and of the conductivity of the system in the ballistic regime.

For neutral particles with spin, an analog of the Aharonov-Bohm phase is represented by the geometric Berry phase. The latter appears if an effective magnetic field responsible for the energy splitting of the two components of a spinor changes smoothly its direction along the ring. In the adiabatic approximation when the spin follows the direction of the magnetic field the phase acquired by a particle during one cycle of the propagation along the ring is equal to half of the solid angle covered by the vector of an effective magnetic field. The geometric phase was experimentally detected in photonic interferometers [7,8] and predicted to play a substantial role in excitonic [9] and polaritonic [10] ring resonators. The latter system will be the focus of our attention in the present Rapid Communication.

Cavity polaritons are hybrid light-matter quasiparticles emerging in the regime of the strong coupling between the excitonic resonance and the photonic mode of the planar semiconductor microcavity [11]. Compared to purely photonic or purely excitonic systems polaritonic systems have several important advantages. From their photonic component polaritons inherit extremely small effective mass (about 10^{-5} of the mass of free electrons) and large coherence length (on the millimeter scale) [12]. On the other hand, the presence of the excitonic component results in polariton-polariton interactions,

which can be controlled by means of external electromagnetic fields [13].

An important property of cavity polaritons is their spin (or pseudospin) [14], inherited from the spins of quantum well excitons and cavity photons. Similar to photons, polaritons have two possible spin projections on the structure growth axis corresponding to two opposite circular polarizations. States with opposite spins can be mixed by effective magnetic fields of various origins. A magnetic field applied along the structure growth axis and acting on the excitonic component splits energies of the spin positive and spin negative polariton states, whereas TE-TM splitting of the photonic modes hybridizes these states via the linear coupling [14]. Because of the effective spin-orbit interaction it provides to polaritonic systems [15–17], TE-TM splitting has recently been shown to play an important role in various types of phenomena in artificial lattices [18–27].

The polariton interactions render the system nonlinear and enable the propagation of self-sustained nonlinear entities (i.e., solitons) whose properties depend significantly on the underlying topology. The importance of topological solitons has been known in several sub-areas of nonlinear field theory including nonlinear optics and cold atom physics, see, e.g., Refs. [28,29]. Their robustness is topologically protected that makes them both attractive for potential applications and readily observable in experiments even in the presence of unavoidable dissipation. Effects of balancing between pump and loss have also been studied in the context of topological localized structures, see, e.g., Ref. [30]. Recently *chiral* effects in nonlinear spinor field models have attracted attention in the context of information processing in quasiconservative, gain, and pump-free systems [31–33] as well as in the dissipative models with pumps [34]. In our recent paper [35], we analyzed how the combination of the effects of the geometric phase and spin-dependent polariton-polariton interactions affects stationary nonlinear states in the polariton rings. On the other hand, it is well known that one-dimensional (1D) polariton

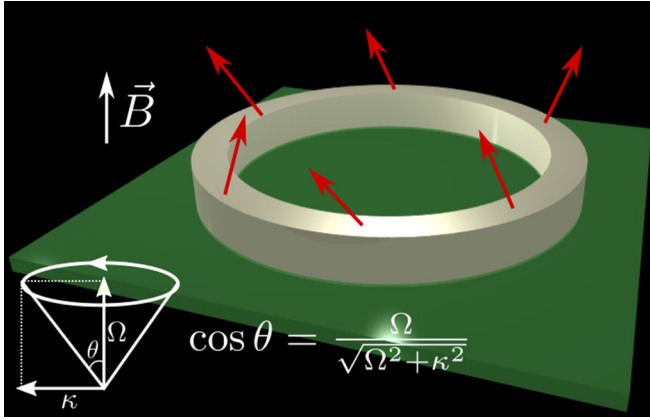


FIG. 1. Schematic of the considered geometry. The polariton ring is placed into external magnetic-field \mathbf{B} perpendicular to its interface. The total effective magnetic field acting on the polariton's spin is a combination of the real magnetic field and the field provided by TE-TM splitting. The direction of the total effective magnetic field changes along the ring as is shown by the arrows. If one moves along the ring it covers a cone characterized by angle θ .

systems support a wide variety of propagating topological defects [36] including solitons and half solitons [37], analogs of magnetic monopoles [38], propagating domain walls [39], and others. The goal of the present Rapid Communication is to analyze *rotating* nonlinear solutions in 1D spinor polariton rings which can be readily realized in practical devices [40].

The model. Interacting spinor polaritons trapped in a quasi-one-dimensional ring resonator (see Fig. 1) can be described by the following system of dimensionless Gross-Pitaevskii equations [35]:

$$i\dot{\psi}_{\pm} = -\partial_{\varphi}^2 \psi_{\pm} + (|\psi_{\pm}|^2 + \alpha|\psi_{\mp}|^2)\psi_{\pm} \pm \Omega\psi_{\pm} + \kappa e^{\mp 2i\varphi} \psi_{\mp}. \quad (1)$$

Here, ψ_{\pm} 's are the components of the exciton-polariton spinor wave-function $\psi \equiv \{\psi_+, \psi_-\}$ in the basis of circular polarizations satisfying $\psi_{\pm}(t, \varphi) = \psi_{\pm}(t, \varphi + 2\pi)$, parameter $\alpha < 0$ characterizes attractive interaction of the cross-polarized polaritons, Ω is half of the Zeeman energy splitting proportional to the amplitude of the applied magnetic field, and κ is half of the momentum-independent TE-TM energy splitting. Parameters Ω and κ are dimensionless and scale in units of $\hbar^2/(2m^*R^2)$, where R is the ring radius and m^* is the exciton-polariton effective mass. Unit energy $\hbar^2/(2m^*R^2)$ can be varied in a broad range. Depending on the detuning between the photon and the exciton frequencies, it can take values from 4 to 40 μeV for a ring radius of 5 μm [35]. TE-TM splitting can be performed both as high as ~ 1 meV in a waveguide of width 1 μm [41,42] and negligibly small by choosing large ring widths. Also, TE-TM splitting can be controlled by changing detuning [43] and the properties of the distributed Bragg reflector [44]. With the unit energy of 40 μeV and the angular velocity of $\omega \sim 1$ it will take about 100 ps for a soliton to circle around the ring, which is on the order of the polariton's lifetime. Normalized densities ψ_{\pm} scale out the polariton interaction constant (which can be on the order of $\sim 10^{-5}$ meV mm $^{-2}$ [45]), and coefficient α is the ratio of interactions between

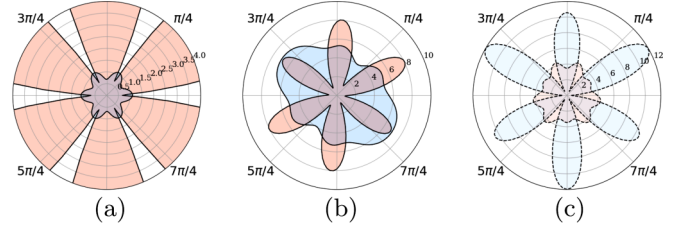


FIG. 2. Different types of rotating solitons at $\alpha = -0.05$, $\rho = 10$, $\kappa = 0.8$, $\Omega = 0.5$, $\omega = 0.4$. The pink (blue) color denotes the density of the ψ_+ (ψ_-) component. (a) and (b) The saturated colors with the solid lines and (c) the dull colors with the dashed lines mark the linearly stable and unstable configurations, respectively.

polaritons with parallel and antiparallel spins, which is a small negative constant [45] (it can also be controlled by the detuning between exciton and photon modes [46]). System (1) describes quasiconservative nonlinear dynamics of exciton-polaritons which has been observed in several experiments [47,48]. It is expected that the unavoidable (small) losses will limit the lifetime of the solitons but will not inhibit their chiral properties discussed in what follows.

To find rotating solutions we switch from the laboratory frame to the frame of reference rotating with frequency ω , which is achieved by replacing the polar angle φ with a new variable $x = \varphi - \omega t$. Seeking the wave functions in the form of $\psi_{\pm}(t, \varphi) = u_{\pm}(t, x)e^{-i\mu t \mp i\varphi}$, where $u_{\pm}(t, x)$'s satisfy periodic boundary conditions: $u_{\pm}(t, x) = u_{\pm}(t, x + 2\pi)$, we get the following system:

$$i\dot{u}_{\pm} = (\hat{D}_{\pm} + |u_{\pm}|^2 + \alpha|u_{\mp}|^2)u_{\pm} + \kappa u_{\mp}, \quad (2)$$

where $\hat{D}_{\pm} = -\mu + i\omega\partial_x - (\partial_x \mp i)^2 \pm \Omega$. Nonlinear spinor systems similar to that in Eq. (2) have been considered earlier in the context of birefringent optical fibers [49,50] and, more recently, for modeling of matter waves in spin-orbit coupled Bose-Einstein condensates [51,52]. Chemical potential μ and frequency ω uniquely select the polariton density integral $\rho \equiv \frac{1}{2\pi} \int_0^{2\pi} (|\psi_+|^2 + |\psi_-|^2) d\varphi$ for a given solution.

We compute rotating solutions by the numerical continuation from the analytically tractable limit $\kappa = \Omega = \omega = \alpha = 0$, where Eq. (2) decouples into a pair of nonlinear Schrödinger equations (NLSEs) whose solutions can be found in terms of Jacobi elliptic functions [53]. Proceeding in this way, we have discovered that system (2) supports a rich variety of nonlinear rotating patterns. We mention here three classes of those. First, when the initial condensate state is chosen to be periodic in one component and exactly zero in the second component, the numerical iterative procedure converges to a solution such that the amplitude of one component is much larger than that of the other one, i.e., either $|\psi_+| \gg |\psi_-|$ or $|\psi_-| \gg |\psi_+|$, see Fig. 2(a). Since the smaller component can be neglected, the properties of this family can be recovered from the scalar NLSE equation. Starting from an initial state with a periodic profile in one component and constant and nonzero density in another one, we obtain a class of solutions where one of the components has a strongly modulated amplitude with pronounced density humps and dips, whereas the other one is modulated relatively weakly, see Figs. 2(b) and 2(c). In the third family, which is the focus of our attention here,

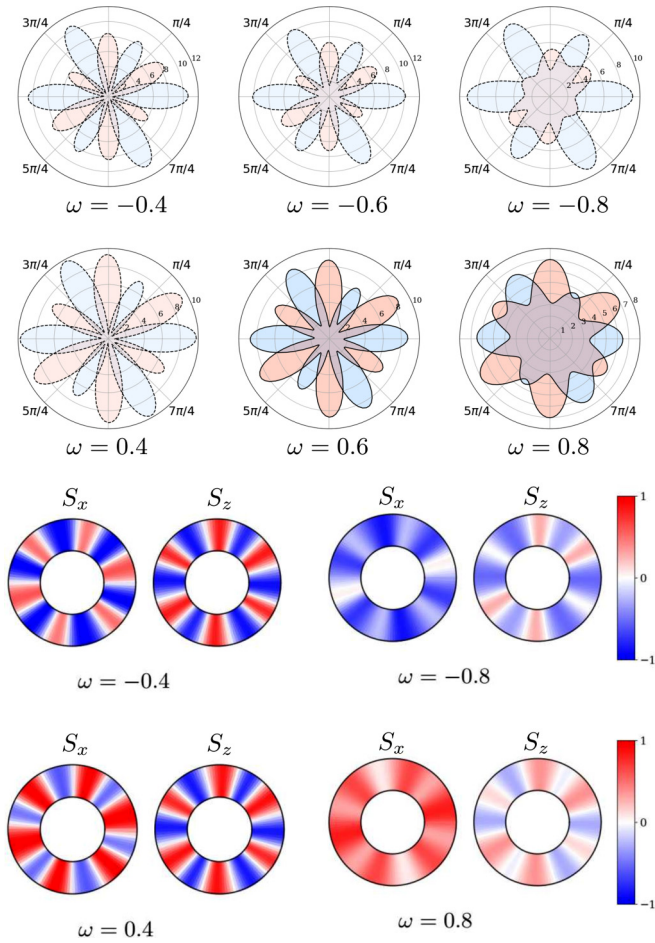


FIG. 3. Six upper panels: several representatives of a family of solutions of type (iii) with $\alpha = -0.05$, $\rho = 10$, $\kappa = 0.8$, and $\Omega = 0.5$ at different angular velocities ω . The unstable solutions are marked by the dull colors and the dashed lines. The linearly stable configurations are marked by the saturated colors and the solid lines. The lower panels show pseudocolor visualizations of Stokes parameters S_x and S_z for $\omega = \pm 0.4$ and $\omega = \pm 0.8$.

initial states with nontrivial periodic densities in both ψ_+ and ψ_- lead to solutions where both components feature strong density modulation, see Fig. 3. The simplest solution, such as this, features two density dips and two density humps. In general, they can have arbitrarily large but always even numbers of petals. Every density dip in this class of solutions corresponds to the π -phase shift, and therefore an even number of them is required to satisfy the periodic boundary conditions. In what follows, we illustrate the main results of our Rapid Communication using the solutions with six petals. However, we have checked that our observations and conclusions also remain valid for smaller and larger numbers of petals.

Chiral solitons. Now we proceed to the *main results* of our Rapid Communication. With the focus on rotating patterns, it is of obvious interest to investigate if and how their properties are affected by the angular velocity ω . To answer this question, in the six upper panels of Fig. 3 we show representative solutions of the third class with six dip-hump pairs. The solutions in the different panels differ by their angular velocities ω . One interesting feature immediately visible in these panels is that

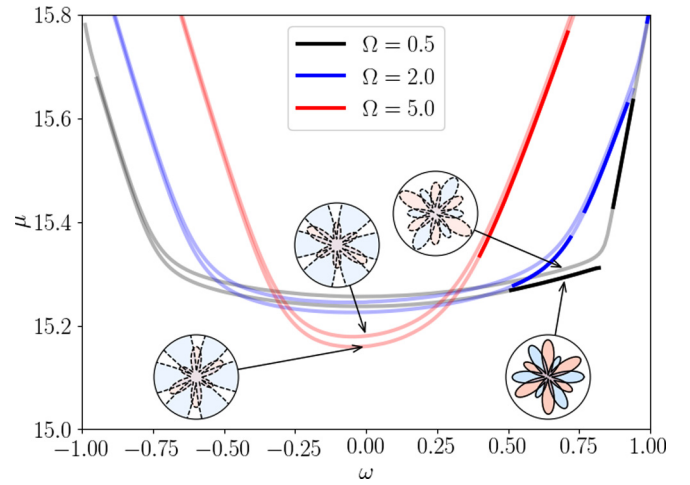


FIG. 4. Dependencies of the chemical potential μ on the rotation velocity ω at different values of the magnetic-field Ω . Several configurations of solitons are shown in the insets. For each set of parameters, two families of rotating solutions arise which differ by the phase difference between the two circularly polarized components. Fragments with the saturated and dull colors correspond to the stable and unstable solutions, respectively. Here $\alpha = -0.05$, $\rho = 10$, and $\kappa = 0.8$.

the increase in the magnitude of velocity can be favorable for the solution's stability: For instance, the unstable solution with $\omega = 0.4$ becomes stable as the velocity increases to $\omega = 0.6$ and, furthermore, to $\omega = 0.8$. Even more interestingly, from Fig. 3 we observe that solitons propagating with opposite velocities (ω and $-\omega$) have essentially different shapes and, generally speaking, different stability properties. For instance, the unstable solution rotating in the counterclockwise direction with velocity $\omega = -0.6$ becomes stable as the rotation's direction is switched to clockwise ($\omega = 0.6$). This means that the found solitons are inherently *chiral* in the sense that solitons propagating with angular velocities of equal amplitudes but opposite directions are not equivalent. In order to highlight additionally the differences in the structures of solitons propagating with opposite velocities, in the lower panels of Fig. 3 we compare pseudocolor plots of Stokes parameters defining the distribution of the linear and circular polarization degrees along the ring for two pairs of counterpropagating patterns,

$$S_x = \frac{2 \operatorname{Re}(\psi_+^* \psi_-)}{|\psi_+|^2 + |\psi_-|^2}, \quad S_z = \frac{|\psi_+|^2 - |\psi_-|^2}{|\psi_+|^2 + |\psi_-|^2}.$$

To demonstrate that the revealed chirality does not depend on the particular choice of the parameters, in the lower panel of Fig. 4 we plot several dependencies of the chemical potential μ on the rotation velocity ω at different nonzero values of the magnetic-field Ω . For each value of Ω , the upper line and lower lines are two different types of solutions which differ by phases of the two circularly polarized components (cf. symmetric and antisymmetric constant amplitude solutions in Ref. [35]). All the obtained dependencies are not symmetric with respect to the vertical axis $\omega = 0$ and consist of unevenly distributed subfamilies of stable and unstable solutions, which is more clear evidence of the solitons' chirality. Additionally, in Fig. 5 we show the dependence of the chemical potential μ on the

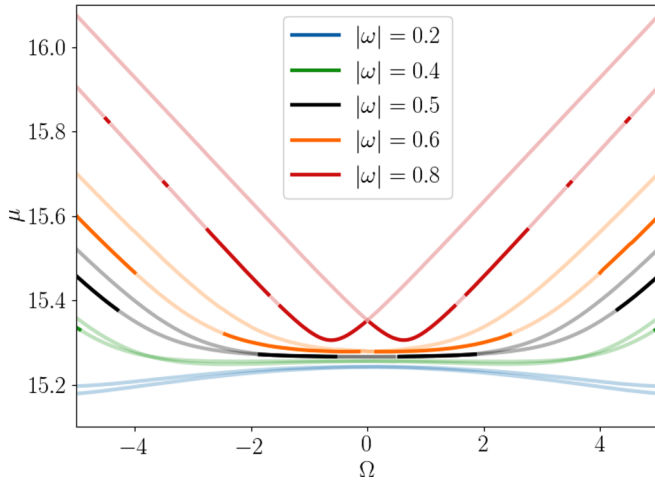


FIG. 5. Dependencies of the chemical potential on the magnetic-field Ω for solitons in Fig. 4. Fragments with the saturated and dull colors correspond to the stable and unstable solutions, respectively.

magnetic-field Ω for solitons in Fig. 4. For every considered velocity, the curves with ω and $-\omega$ intersect exactly at $\Omega = 0$. As another remarkable feature, we note that at rotation velocities $\omega = \pm 0.5$ the solitons exhibit the topological spin-Meissner effect [35] in the region of $|\Omega| \lesssim 2$ when the energies are almost independent of the magnetic field.

To understand the role of external magnetic field, we notice that if the Zeeman splitting is absent [i.e., $\Omega = 0$ in (2)], then a soliton propagating with velocity ω always has a twin propagating with the opposite velocity $-\omega$. Both these counterpropagating solitons have identical properties, i.e., one can be rendered to another by inverting the spatial direction from x to $-x$ and swapping the polarizations—these transformations obviously do not alter the physical properties of the solution. In the meantime, nonzero Ω breaks this symmetry and implies that solitons propagating with two opposite velocities ω and $-\omega$ have different properties. However, if reversing the velocity is accompanied by the change in the magnetic field from Ω to $-\Omega$, then the system becomes invariant under an evident symmetry: Indeed, if $u_+(x)$ and $u_-(x)$ are time-independent solutions of Eq. (2), then a pair of new functions $U_+(x) = u_-(-x)$ and $U_-(x) = u_+(-x)$ solves the same system with $\omega \rightarrow -\omega$, $\Omega \rightarrow -\Omega$.

The chiral nature of the solitons is linked with breaking of the time-inversion symmetry which appears naturally in the systems with present gauge fields. It can be shown that in the system we consider that a synthetic $U(1)$ gauge field appears due to the combination of TE-TM splitting and an external magnetic field acting on the polariton spin. Indeed, let us consider the projection of the original system of the equations onto the lowest-energy spin state in adiabatic approximation [54]. Diagonalizing the Hamiltonian associated with system

(1) in the basis of dressed states, one observes that in the limit of small densities $|\psi_{\pm}| \ll 1$ the adiabatic dynamics is governed by the following effective density-dependent Hamiltonian [55]: $\hat{H} = (\hat{p} - A)^2 + g|\psi_1|^2$, where $\hat{p} = -i\partial_\varphi$ is the momentum operator, $|\psi_1|^2$ is the local squared density of the ψ_+ component in one of the dressed states, and g is the effective nonlinearity coefficient (see the Supplemental Material [56]),

$$g = \frac{2\Omega^2 + \kappa^2(\alpha + 1)}{\Lambda(\Lambda + \Omega)} - \frac{(1 - \alpha)\kappa^2\Omega}{\Lambda^4}, \quad (3)$$

where $\Lambda = \sqrt{\kappa^2 + \Omega^2}$. The geometric density-dependent gauge field reads

$$A = (\Omega\Lambda^{-1} - 1) + (1 - \alpha)\Omega\Lambda^{-2}(1 - \Omega\Lambda^{-1})|\psi_1|^2. \quad (4)$$

The appearance of the gauge field can be qualitatively explained in the following way. Suppose that the polariton is moving adiabatically along the ring. If spin-dependent polariton-polariton interactions are neglected, the direction of the total effective magnetic field acting on the polariton's spin changes along the ring according to the formula $\mathbf{B} = \mathbf{e}_x\kappa \cos 2\varphi + \mathbf{e}_y\kappa \sin 2\varphi + \mathbf{e}_z\Omega$ (see Fig. 1). In the adiabatic approximation the spin follows the direction of the magnetic field, and therefore when the polariton completes one round of the propagation along the ring its spin covers a nonzero solid angle which leads to the appearance of the geometric phase equivalent to

$$2\pi(\cos \theta - 1) = 2\pi(\Omega/\Lambda - 1) = \int_0^{2\pi} A d\varphi. \quad (5)$$

From this expression one immediately deduces the first term in Eq. (4) corresponding to the linear regime.

To conclude, in this Rapid Communication we have introduced a class of solitons which have the form of localized defects rotating with constant angular velocity in a spinor polariton ring. The properties of the solitons, such as the spatial shape and the dynamical stability, can be effectively managed by the angular velocity. The solitons feature a chiral nature which makes the solutions propagating in the clockwise and counterclockwise directions not equivalent. The chirality is explained using the concept of effective gauge field stemming from the combined effect of the TE-TM splitting and the external magnetic field.

Acknowledgments. We thank Dr. I. V. Iorsh for valuable discussions and the preparation of Fig. 1. This Rapid Communication was supported by Megagrant No. 14.Y26.31.0015 and Goszadaniy No. 3.8884.2017/8.9 and No. 3.2614.2017/4.6 of the Ministry of Education and Science of Russian Federation. I.A.S acknowledges support from the Icelandic Research Fund, Grant No. 163082-051. D.V.S. acknowledges support from the Royal Society and ITMO University Visiting Professorship via the Government of Russia Grant 074-U01.

- [1] H. Eschrig, *Topology and Geometry for Physics* (Springer, Berlin, 2011).
 [2] A. G. Aronov and Y. V. Sharvin, *Rev. Mod. Phys.* **59**, 755 (2004).

- [3] S. Viefers, P. Koskinen, P. Singha Deo, and M. Manninen, *Physica E* **21**, 1 (2004).
 [4] T. Ihn, A. Fuhrer, L. Meier, M. Sigrist, and K. Ensslin, *Europhys. News* **36**, 78 (2005).

- [5] W. Ehrenberg and R. E. Siday, *Proc. Phys. Soc., London, Sect. B* **62**, 8 (1949).
- [6] Y. Aharonov and D. Bohm, *Phys. Rev.* **115**, 485 (1959).
- [7] A. Tomita and R. Y. Chiao, *Phys. Rev. Lett.* **57**, 933 (1986).
- [8] P. G. Kwiat and R. Y. Chiao, *Phys. Rev. Lett.* **66**, 588 (1991).
- [9] K. Mouloupoulos and M. Constantinou, *Phys. Rev. B* **70**, 235327 (2004).
- [10] I. A. Shelykh, G. Pavlovic, D. D. Solnyshkov, and G. Malpuech, *Phys. Rev. Lett.* **102**, 046407 (2009).
- [11] H. Deng, H. Haug, and Y. Yamamoto, *Rev. Mod. Phys.* **82**, 1489 (2010).
- [12] D. Ballarini, D. Caputo, C. S. Muñoz, M. De Giorgi, L. Dominici, M. H. Szymańska, K. West, L. N. Pfeiffer, G. Gigli, F. P. Laussy, and D. Sanvitto, *Phys. Rev. Lett.* **118**, 215301 (2017).
- [13] T. C. H. Liew, I. A. Shelykh, and G. Malpuech, *Physica E* **43**, 1543 (2011).
- [14] I. A. Shelykh, A. V. Kavokin, and G. Malpuech, *Phys. Status Solidi B* **242**, 2271 (2005).
- [15] A. Kavokin, G. Malpuech, and M. Glazov, *Phys. Rev. Lett.* **95**, 136601 (2005).
- [16] C. Leyder, M. Romanelli, J. P. Karr, E. Giacobino, T. C. H. Liew, M. M. Glazov, A. V. Kavokin, G. Malpuech, and A. Bramati, *Nat. Phys.* **3**, 628 (2007).
- [17] V. G. Sala, D. D. Solnyshkov, I. Carusotto, T. Jacqmin, A. Lemaître, H. Terças, A. Nalitov, M. Abbarchi, E. Galopin, I. Sagnes, J. Bloch, G. Malpuech, and A. Amo, *Phys. Rev. X* **5**, 011034 (2015).
- [18] T. Jacqmin, I. Carusotto, I. Sagnes, M. Abbarchi, D. D. Solnyshkov, G. Malpuech, E. Galopin, A. Lemaître, J. Bloch, and A. Amo, *Phys. Rev. Lett.* **112**, 116402 (2014).
- [19] K. Kusudo, N. Y. Kim, A. Löffler, S. Höfling, A. Forchel, and Y. Yamamoto, *Phys. Rev. B* **87**, 214503 (2013).
- [20] M. Milićević, T. Ozawa, P. Andreakou, I. Carusotto, T. Jacqmin, E. Galopin, A. Lemaître, L. Le Gratiet, I. Sagnes, J. Bloch, and A. Amo, *2D Mater.* **2**, 034012 (2015).
- [21] D. D. Solnyshkov, A. V. Nalitov, and G. Malpuech, *Phys. Rev. Lett.* **116**, 046402 (2016).
- [22] D. R. Gulevich, D. Yudin, I. V. Iorsh, and I. A. Shelykh, *Phys. Rev. B* **94**, 115437 (2016).
- [23] O. Bleu, D. D. Solnyshkov, and G. Malpuech, *Phys. Rev. B* **95**, 115415 (2017).
- [24] D. R. Gulevich, D. Yudin, D. V. Skryabin, I. V. Iorsh, and I. A. Shelykh, *Sci. Rep.* **7**, 1780 (2017).
- [25] O. Bleu, D. D. Solnyshkov, and G. Malpuech, *Phys. Rev. B* **95**, 235431 (2017).
- [26] D. R. Gulevich and D. Yudin, *Phys. Rev. B* **96**, 115433 (2017).
- [27] C. E. Whittaker, E. Cancellieri, P. M. Walker, D. R. Gulevich, H. Schomerus, D. Vaitiekus, B. Royall, D. M. Whittaker, E. Clarke, I. V. Iorsh, I. A. Shelykh, M. S. Skolnick, and D. N. Krizhanovskii, *Phys. Rev. Lett.* **120**, 097401 (2018).
- [28] N. Manton and P. Sutcliffe, *Topological Solitons* (Cambridge University Press, Cambridge, UK, 2007).
- [29] Y. S. Kivshar and G. P. Agrawal, *Optical Solitons* (Academic, San Diego, 2003).
- [30] Y. V. Kartashov, C. Hang, G. Huang, and L. Torner, *Optica* **3**, 1048 (2016).
- [31] S. Cheon, T.-H. Kim, S.-H. Lee, and H. W. Yeom, *Science* **350**, 182 (2015).
- [32] T.-H. Kim, S. Cheon, and H. W. Yeom, *Nat. Phys.* **13**, 444 (2017).
- [33] Y. V. Kartashov and D. V. Skryabin, *Optica* **3**, 1228 (2016).
- [34] Y. V. Kartashov and D. V. Skryabin, *Phys. Rev. Lett.* **119**, 253904 (2017).
- [35] D. R. Gulevich, D. V. Skryabin, A. P. Alodjants, and I. A. Shelykh, *Phys. Rev. B* **94**, 115407 (2016).
- [36] M. Sich, D. V. Skryabin, and D. N. Krizhanovskii, *C. R. Phys.* **17**, 908 (2016).
- [37] H. Flayac, D. D. Solnyshkov, and G. Malpuech, *Phys. Rev. B* **83**, 193305 (2011).
- [38] R. Hivet, H. Flayac, D. D. Solnyshkov, D. Tanese, T. Boulier, D. Andreoli, E. Giacobino, J. Bloch, A. Bramati, G. Malpuech, and A. Amo, *Nat. Phys.* **8**, 724 (2012).
- [39] T. C. H. Liew, A. V. Kavokin, and I. A. Shelykh, *Phys. Rev. Lett.* **101**, 016402 (2008).
- [40] G. Liu, D. W. Snoke, A. Daley, L. N. Pfeiffer, and K. West, *Proc. Natl. Acad. Sci. USA* **112**, 2676 (2015).
- [41] A. Kuther, M. Bayer, T. Gutbrod, A. Forchel, P. A. Knipp, T. L. Reinecke, and R. Werner, *Phys. Rev. B* **58**, 15744 (1998).
- [42] G. Dasbach, C. Diederichs, J. Tignon, C. Ciuti, P. Roussignol, C. Delalande, M. Bayer, and A. Forchel, *Phys. Rev. B* **71**, 161308 (2005).
- [43] S. Dufferwiel, F. Li, E. Cancellieri, L. Giriunas, A. A. P. Trichet, D. M. Whittaker, P. M. Walker, F. Fras, E. Clarke, J. M. Smith, M. S. Skolnick, and D. N. Krizhanovskii, *Phys. Rev. Lett.* **115**, 246401 (2015).
- [44] G. Panzarini, L. C. Andreani, A. Armitage, D. Baxter, M. S. Skolnick, V. N. Astratov, J. S. Roberts, A. V. Kavokin, M. R. Vladimirova, and M. A. Kaliteevski, *Phys. Rev. B* **59**, 5082 (1999).
- [45] T. C. H. Liew, A. V. Kavokin, and I. A. Shelykh, *Phys. Rev. B* **75**, 241301(R) (2007).
- [46] M. Vladimirova, S. Cronenberger, D. Scalbert, K. V. Kavokin, A. Miard, A. Lemaître, J. Bloch, D. Solnyshkov, G. Malpuech, and A. V. Kavokin, *Phys. Rev. B* **82**, 075301 (2010).
- [47] A. Amo, S. Pigeon, D. Sanvitto, V. G. Sala, R. Hivet, I. Carusotto, F. Pisanello, G. Lemenager, R. Houdre, E. Giacobino, C. Ciuti, and A. Bramati, *Science* **332**, 1167 (2011).
- [48] P. M. Walker, L. Tinkler, D. V. Skryabin, A. Yulin, B. Royall, I. Farrer, D. A. Ritchie, M. S. Skolnick, and D. N. Krizhanovskii, *Nat. Commun.* **6**, 8317 (2015).
- [49] B. A. Malomed, *Phys. Rev. A* **43**, 410 (1991).
- [50] N. Akhmediev and A. Ankiewicz, *Solitons: Nonlinear Pulses and Beams* (Springer, Berlin, 1997).
- [51] V. Achilleos, D. J. Frantzeskakis, P. G. Kevrekidis, and D. E. Pelinovsky, *Phys. Rev. Lett.* **110**, 264101 (2013); V. Achilleos, J. Stockhofe, P. G. Kevrekidis, D. J. Frantzeskakis, and P. Schmelcher, *Europhys. Lett.* **103**, 20002 (2013).
- [52] O. Fialko, J. Brand, and U. Zülicke, *Phys. Rev. A* **85**, 051605(R) (2012); C. Zhang, *ibid.* **95**, 033612 (2017).
- [53] L. D. Carr, C. W. Clark, and W. P. Reinhardt, *Phys. Rev. A* **62**, 063610 (2000).
- [54] J. Dalibard, F. Gerbier, G. Juzeliūnas, and P. Öhberg, *Rev. Mod. Phys.* **83**, 1523 (2011).
- [55] R. J. Dingwall, M. Edmonds, J. Helm, B. A. Malomed, and P. Öhberg, *New J. Phys.* (2018), doi: [10.1088/1367-2630/aab29e](https://doi.org/10.1088/1367-2630/aab29e).
- [56] See Supplemental Material at <http://link.aps.org/supplemental/10.1103/PhysRevB.97.161302> for the detailed derivation of the density-dependent adiabatic Hamiltonian.